

DERIVATED TURBULENCE MODEL TO PREDICT HARMONIC LOADS IN TRANSONIC SEPARATED FLOWS OVER A BUMP

M. Philit^{1*}, P. Ferrand¹, S. Labit², J-C Chassaing², S. Aubert³, T. Fransson⁴

¹ UMR CNRS 5509, Université de Lyon, LMFA, Ecole Centrale de Lyon, France

² Université Pierre et Marie Curie, Institut Jean Le Rond d'Alembert, France

³ FLUOREM SAS, France

⁴ Department of Heat and Power Technology, Royal Institute of Technology, Sweden

Keywords: *Linearized RANS, Turbulence, Shock Wave/Boundary Layer Interaction*

Abstract

Nowadays, frequency-domain time-linearized flow solvers are widely employed for aerospace engineering applications like turbomachinery or wing aeroelasticity. Due to substantial savings in the computational costs compared to the classical time-nonlinear methods, these methods are promising in the context of industrial design process in aeronautics. Nevertheless, the time-linearized solution is often relying on the assumption of frozen turbulence which can lead to significant discrepancies in the unsteady flow prediction, especially when the steady flow exhibits strong shock-wave boundary layer interactions. In the present paper, we propose to account for effects of the turbulence on the unsteady field by linearizing the k - ω turbulence closure of Wilcox. To this end, an Automatic Derivation Tool is applied to the discretized Reynolds Average Navier-Stokes solver Turb'FlowTM. The resulting time-linearized LRANS solver Turb'LinTM is used to compute the unsteady response of forced shock-wave motion in a transonic nozzle due to harmonic back pressure fluctuations. The accuracy of the present methodology is assessed by comparison with time-nonlinear and harmonic-balance solutions for both weak and strong shock-wave turbulent boundary layer interactions forced by an excitation frequency equal to 500 Hz.

1 Introduction

Important progresses have been made during the last decades in the development of time-linearized solvers for a wide range of unsteady time-periodic flows ([1],[2],[3]). Compared to the conventional time non-linear Reynolds-Averaged Navier-Stokes methods (URANS), such frequency-domain based approaches combine high computational time efficiency with a high level of accuracy at high excitation frequencies. For these reasons, the time-linearized methods are very popular for aeronautical engineering problems where flow unsteadiness is characterized by harmonic oscillations with small amplitudes. However, it is well known that these approaches suffer from a lack of robustness and accuracy when strong local non-linear effects are present in the underlying steady problems as for instance, transonic nozzle configurations with flow separations. The main reason of this loss of accuracy is due to the fact that most of time-linearized solvers assume that the turbulence is frozen to the steady state during the unsteady computations. Obviously, this drawback can be raised by using an harmonic balance approach [4, 5] which naturally accounts for unsteady perturbations in the turbulent eddy viscosity by means of several coupled pseudo-steady flows. In this work, a different approach is investigated by means of the linearization of the k -

ω turbulence model ([6]) employed for the computation of the steady flow. As a consequence, this formulation can be employed in the context of both time-linearized flows and gradient-based approaches for aerodynamic design optimization.

2 Time-linearized Navier-Stokes methodology (LRANS)

The flow is modelled by the Reynolds-Averaged Navier-Stokes equations (RANS). A finite volume method is employed to discretize the governing equations on a structured multiblock grid

$$\frac{d}{dt}(\mathbf{J}(\mathbf{p}) \mathbf{q}) + \mathbf{F}(\mathbf{p}, \mathbf{q}) = \mathbf{0} \quad (1)$$

where \mathbf{q} is the vector of nodal conservative and turbulent variables, \mathbf{J} denotes the vector of mesh cells volume, \mathbf{p} is the vector determining boundary conditions, \mathbf{F} is the non-linear function expressing the balance of convective and viscous fluxes. In the framework of linear analysis, the imposed instantaneous operating conditions \mathbf{p} and the unknown \mathbf{q} are modelled as :

$$\mathbf{p} = \bar{\mathbf{p}} + \delta\mathbf{p}e^{i\omega t}, \quad (2)$$

$$\mathbf{q} = \bar{\mathbf{q}} + \delta\mathbf{q}e^{i\omega t} \quad (3)$$

where $(\bar{\mathbf{p}}, \bar{\mathbf{q}})$ are the steady state values and $(\delta\mathbf{p}, \delta\mathbf{q})$ are the small perturbation harmonic amplitudes at a prescribed angular frequency ω .

Introducing the previous decomposition in the RANS equations (Eq. [1]) and neglecting high order terms gives an uncoupled system of equations whose unknown is $(\bar{\mathbf{q}}, \delta\mathbf{q})$

$$\mathbf{F}(\bar{\mathbf{q}}, \bar{\mathbf{p}}) = \mathbf{0} \quad (4)$$

$$\left\{ i\omega\mathbf{J}(\bar{\mathbf{p}}) + \frac{\partial\mathbf{F}}{\partial\mathbf{q}}(\bar{\mathbf{q}}, \bar{\mathbf{p}}) \right\} \delta\mathbf{q} = -\frac{\partial\mathbf{F}}{\partial\mathbf{p}}(\bar{\mathbf{q}}, \bar{\mathbf{p}})\delta\mathbf{p} \quad (5)$$

Equation (4) corresponds to the RANS formulation for the steady flow (SRANS). The time-linearized solution (LRANS) is described in the frequency domain by Eq. (5). The most important work in solving the LRANS equations is to compute the jacobian matrices of the flux with respect to $\delta\mathbf{q}$ and $\delta\mathbf{p}$.

3 Computational methods

In this work, the steady flow solution (Eq. 4) and the unsteady non-linear flow solution are computed using the TurbflowTM solver [7, 8]. Spatial discretization is based on the 3rd order ROE FDS scheme with HCUI (Harmonic Cubic Upwind Interpolation) flux limiting. Turbulent equations are discretized using a second order upwind scheme in conjunction with SMARTER (Sharp Monotonic Algorithm for Realistic Transport Equation Revised) limiters [9]. The URANS solver is based on the same spatial discretization. Time-integration is performed using a 5 steps Runge-Kutta scheme.

The LRANS solution (Eq. 5) is computed using the Turb'LinTM software by FLUOREM. Note that, for this case, a spatial central scheme is employed in order to deal efficiently with acoustic predictions. A GMRES Krylov algorithm without pseudo-time is employed to solve the resulting linear system. This approach was found to be more robust than conventional LRANS approaches based on pseudo-time marching [10]. The partial derivatives in Eq. 5 are evaluated exactly by applying an Automatic Differentiation Tool developed by FLUOREM to the \mathbf{F} function (Eq. 1) computed using Turb'Flow. Since the initial purpose of this software was to deal with parametrized steady flow solutions [11, 12], any turbulence model implemented in the underlying RANS solver could be derived. In this study, all computations (if not specified otherwise) are carried out using the $k-\omega$ model ([6]). This model was chosen based on its efficiency to deal with reverse pressure gradient. A limiting procedure is applied in order to ensure the physical meaning of the turbulent kinetic production term. As far as LRANS computations are concerned, we investigate two different approaches. First, we apply the frozen turbulence assumption which means that the time-linearized equations (F.T. LRANS) are solved for the conservative variables only. The second approach, namely the harmonic turbulence RANS method (H.T. LRANS) assumes that the response of the unsteady turbulent field is harmonic.

4 Experimental configuration

The studied experimental configuration ([13],[14]) consists in a transonic nozzle equipped with a two-dimensional bump at its lower wall (Fig. 1). The nozzle geometry is 100 mm wide and 120mm high. The length of the bump is equal to 184 mm. This facility was designed to deal with forced oscillations of shock-wave boundary layer interaction (SWBLi). The setup can be employed to investigate unsteady phenomena commonly observed for turbomachinery applications, like for instance, potential effects or rotor-stator interactions, by imposing periodic back pressure fluctuations downstream of the flow. A rotating elliptical cam is used to generate pressure perturbation up to 500 Hz. The shock-wave is then expected to interact with the boundary layer. This configuration aims to reproduce the SWBLi observed on the suction side of turbomachinery blades near choked flutter operating conditions. For this case, the non-linear interaction between the back-pressure fluctuation and the shock-wave can lead to large oscillations of the aerodynamical force acting on the bump. Accurate prediction of such unsteady loads represents a crucial issue in aeromechanical design of turbomachinery blades in order to prevent aeroelastic instability and flutter.

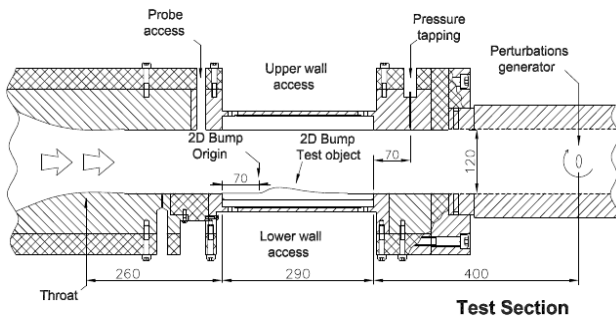


Fig. 1 Test section of the studied experimental facility (Bron [14] 2004)

5 Computation of two-dimensional unsteady flows

5.1 Flow configuration

First, the results are discussed by means of two-dimensional numerical simulations. Both URANS and harmonic balance RANS are used as reference solutions to validate the LRANS computations. The size of the computational domain results from previous numerical studies performed in [13]. The specific heat ratio equals $\gamma = 1.4$ and the perfect gas constant is $R = 287J/kg/K$. The thermal conductivity is assumed constant $k = 2.5410^{-2}m.kg/K.s^3$ while the dynamic viscosity follows the Sutherland law. The thickness of the boundary layer imposed at the inlet is equal to 9 mm. Walls are considered as adiabatic.

Two different operating points (see table 1) were selected in order to highlight the sensitivity of the time-linearized solution in the presence of strong non-linear effect interactions. Both cases use an excitation frequency of 500 Hz.

	P_t^{in}	P_s^{out}	T_t^{in}	δP_s
A	160 kPa	112 kPa	303 K	1.25 kPa
B	160 kPa	106 kPa	303 K	2.12 kPa

Table 1 Description of the operating points employed for two-dimensional unsteady computations with an excitation frequency equal to 500 Hz

5.2 Time non-linear solution

In order to get a better understanding of the effects of turbulence closure and spatial discretization onto the steady flow, a second RANS solver for structured grids was employed in this work (<http://sourceforge.net/projects/aerodynamics/>). The Navier-Stokes equations with near-wall wall-normal-free RSM closure [15, 16] are solved using an implicit upwind-biased discretization, with dual-time-stepping for both steady and unsteady flow configurations [17].

Fig. 2 shows the cartography of the steady Mach number field obtained for the flow configurations depicted in Tab. 1. We clearly observed that the shock-wave extends up to the middle of

the nozzle for case A while the nozzle is entirely choked for case B. Both configurations exhibit a flow separation over the bump whose characteristics are reported in Tab. 2 for the case of the $k-\omega$ and RSM turbulence closures.

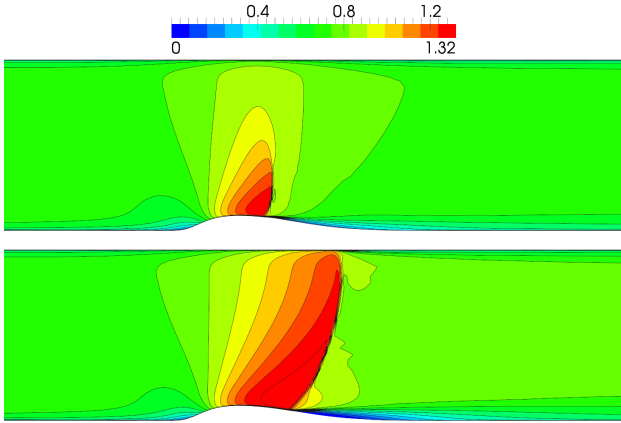


Fig. 2 Mach Number for configuration A (up) and B (down)

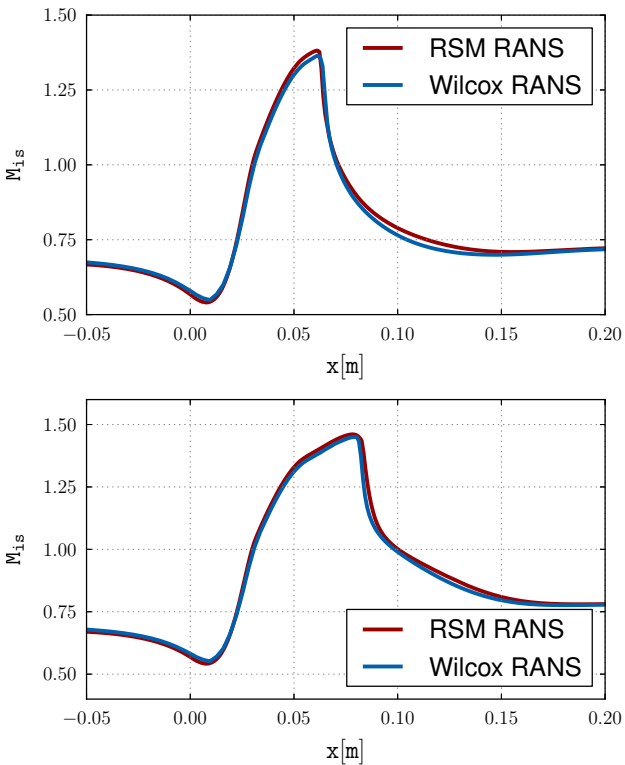


Fig. 3 Isentropic Mach Number on bump wall for configuration A (up) and B (down)

[m]	x_{shock}	$x_{sep.}$	$x_{reatt.}$
Wilcox (A)	0.0627	0.0666	0.0730
Wilcox (B)	0.0809	0.0843	0.1275
RSM (A)	0.0621	0.065	0.075
RSM (B)	0.0835	0.088	0.122

Table 2 Influence of turbulence modeling onto the characteristics of the flow separation regions.

The corresponding isentropic Mach number distributions over the bump are presented in Fig. 3. As far as the case A is concerned, we remark that minors differences between the two methods are observed at the peak of the shock-wave and in the diverging section of the nozzle. In particular, the Mach number at the shock-wave is slightly stronger for the RSM-RANS computations.

Figure 4 presents the distributions of the amplitude and phase of the pressure perturbation obtained for case B (Tab. 1). The time-nonlinear RSM-RANS results were obtained using 360 instants per period for the back-pressure excitation. As expected, we note that the location of the shock-wave strongly affects the unsteady results. These discrepancies, which are observed from $x = 0.09$ to $x = 0.16$ for both the amplitude and phase of the pressure fluctuations, are mainly due to differences in the turbulence closures. In the vicinity of the shock a 40° shift is observed as well as near the reattachment point. We also remark that a constant amplitude of the pressure perturbation is given by the RSM-RANS solution inside the separation region. However, a different shape is observed for the case of the $k-\omega$ turbulence model.

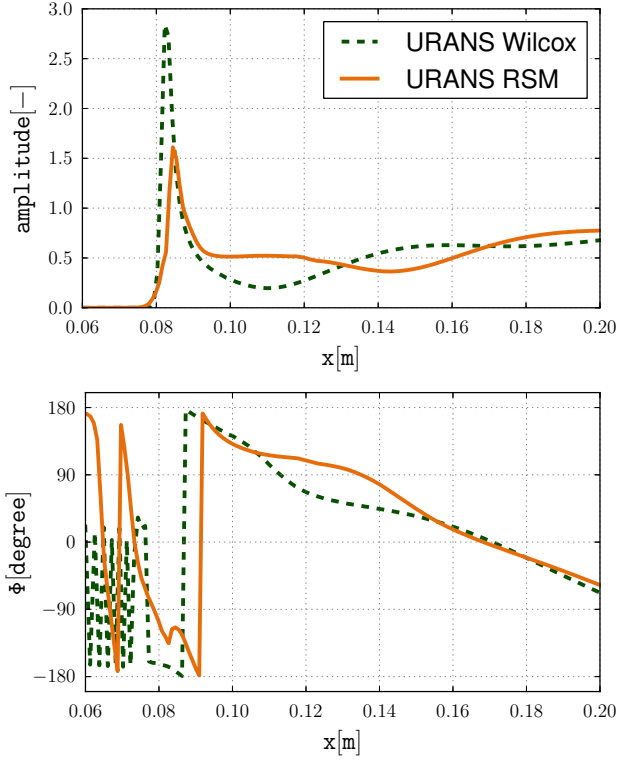


Fig. 4 Pressure fluctuation on bump wall, configuration B

5.3 Analysis of LRANS results

Here, the performance of the LRANS method for capturing unsteady flows is analyzed in great details. First we only focus on LRANS results based on the frozen-turbulence assumption. However, in order to quantify the effect of the steady-state onto the perturbed pressure field, we compare the results obtained using Turb'LinTM with central space discretization to those resulting from an upwind discretization of the time-linearized equations [10] coupled with the RSM-RANS steady flow solver presented in the previous section. As a consequence, we expect to observe similar quantitative difference as those obtained for URANS results. Fig. 5 shows the distribution of the pressure fluctuation for both the lower wall with the bump and the upper wall. We see that the agreement between the LRANS methods is better for the upper wall since the SW-BL interaction is not as strong as those observed over the bump. Again, this is directly related to the computation of the turbulent

steady-field.

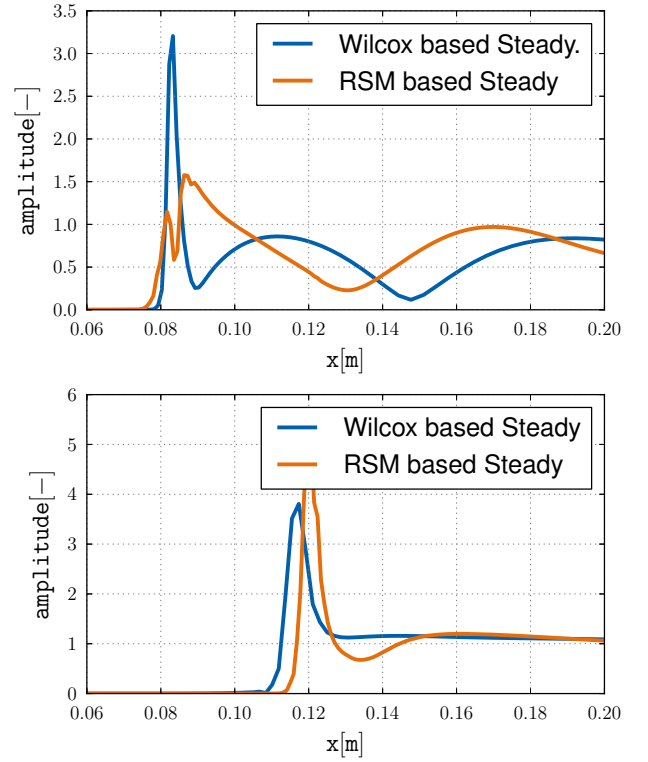


Fig. 5 Normalized pressure fluctuations over the bump (top view) and along the upper wall (down view) obtained for case B (Tab. 1) using upwind or central LRANS methods based on frozen turbulence but with different steady fields

Now, we investigate the importance to account for time-harmonic fluctuations of the turbulent field by means of the Turb'LinTM flow solver. Fig. 6 and 7 show the pressure distribution obtained for case A ($P_s^{out} = 112$ kPa) computed using URANS and LRANS with both Harmonic Turbulence and Frozen Turbulence methods.

Similarly to potential interactions in turbomachines, outlet static pressure fluctuations propagate upstream at a relative velocity $|c - U|$. As long as the propagating speed is unchanged, the slope of the phase angle also remains constant. However in the vicinity of the shock, the phase angle increases corresponding to a downstream propagating evanescent wave. Moreover, we notice that the agreement of the phase distribution is excellent between LRANS and URANS.

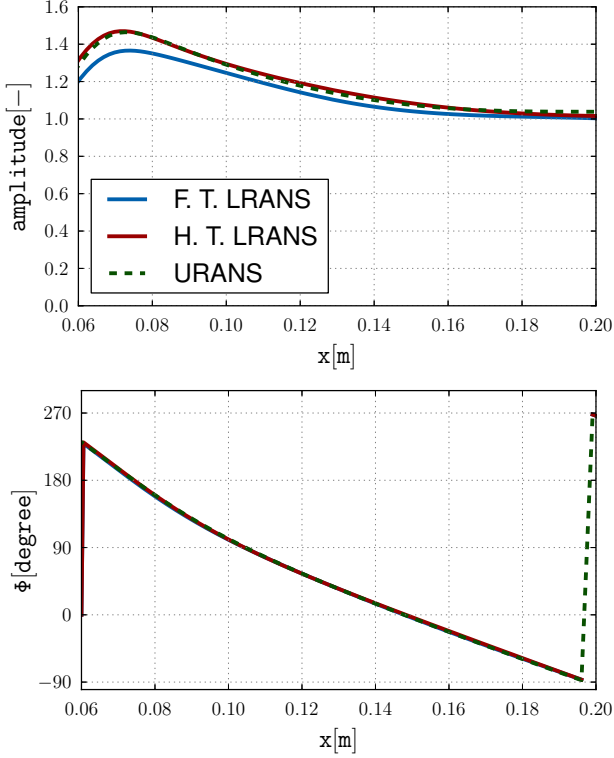


Fig. 6 Normalized Pressure Fluctuations on Upper wall for weak shock (case A)

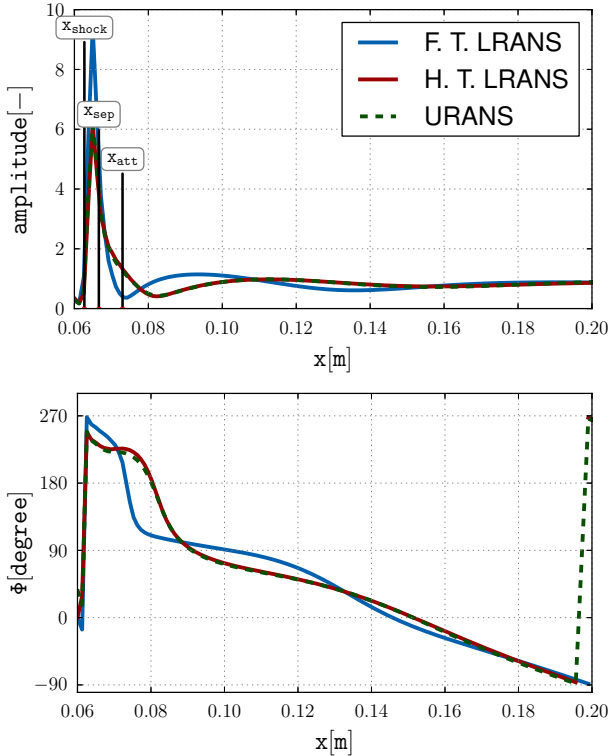


Fig. 7 Normalized Pressure Fluctuations on bump wall for weak shock (case A)

Some discrepancies are visible on the lower

wall where boundary layer effects are more important due to the impact of the shock-wave. These results suggest that for unsteady flows without strong shock boundary layer interaction, the frozen turbulence model gives accurate predictions of the time-linearized pressure field.

Now we examine the results obtained for $P_s^{out} = 106$ kPa at the lower wall (case B, Fig. 9). Before shock position, the phase component was zeroed when it was found too noisy because of low amplitude. In this case, the amplitude of pressure waves is less than those observed for case A (Fig. 7). A possible explanation is that flow gradients involved in the steady flow at $P_s^{out} = 106$ kPa are weakened due to the presence of the flow separation. Thus, the resulting unsteady fluctuations are less significant when the shock-wave oscillates.

We clearly observe on Fig. 9 that results obtained using LRANS with frozen turbulence strongly differ from those computed from H.T. LRANS and URANS. In particular we remark that these discrepancies extend outwards from the separation regions. On the contrary, the agreement of the predictions at the upper wall is satisfying (Fig. 8) since the impinging shock-wave is not strong enough to induce a separated flow.

From a physical point of view, the pressure field at the separation point seems to be in phase with those of the shock position, which means that the flow separation is bounded to the shock motion.

5.4 Non-linear coupling effects

Recall that the LRANS formulation means that the unsteady flow can be decomposed as a small time-harmonic perturbation superimposed to an underlying steady flow. Since we focus in this work to unsteady flows with local strong non-linear interaction, it is interesting to compare the performance of the HT-LRANS with those of an harmonic-balance RSM-RANS formulation (HB-RSM-RANS). This approach, which is based on the Fourier decomposition of the flow variables and residuals was developed from the steady RSM-RANS solver presented in section

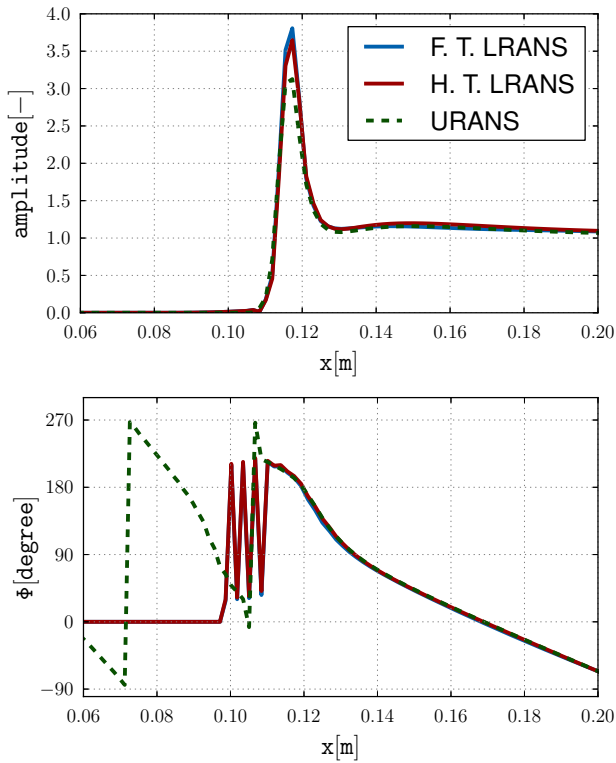


Fig. 8 Normalized Pressure Fluctuations on Upper wall for strong shock (case B)

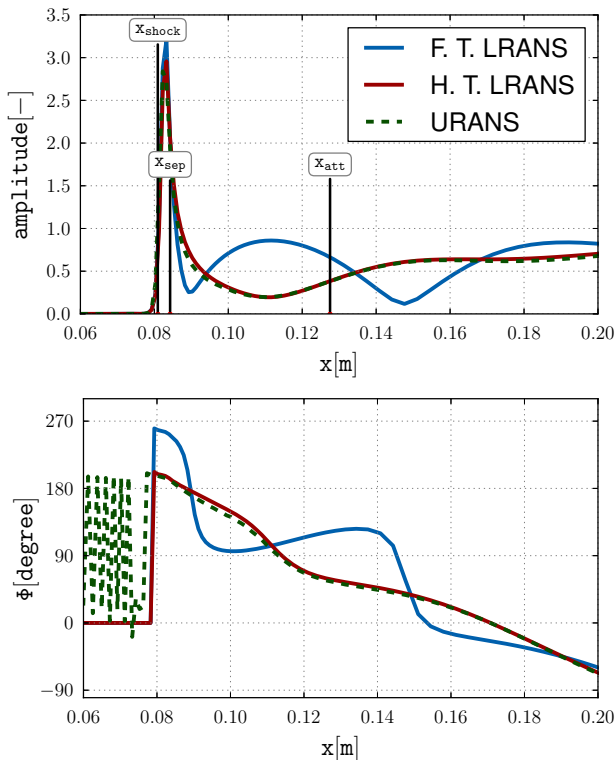


Fig. 9 Normalized Pressure Fluctuations on bump wall for strong shock (case B)

5.2. A Time spectral procedure was implemented for the solution of the harmonic balance equations as described by [4]. The resulting coupled pseudo-steady states are solved using the same spatial and time-integration schemes to those employed for the RSM-RANS solver. Here, a single pressure harmonic was considered in the Fourier decomposition, leading to three pseudo-steady RANS computations. The amplitude of the first pressure harmonic coefficient is compared with the pressure fluctuations obtained from the HT-RANS in Fig. 10. It is very interesting to note that the agreement between the two methods is excellent since different grid sizes and spatial discretization were employed. In particular, the magnitude and the sharpness of the pressure peak agree very satisfactorily. Then we can reasonably conclude that, for this particular flow configuration, the coupling effect of the time-averaged and the 1st harmonic has minor influences onto the unsteady flows.

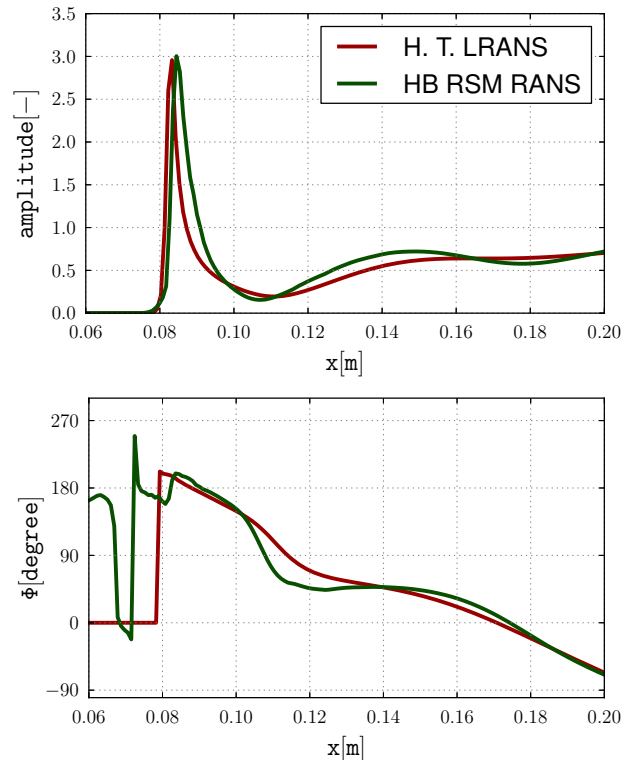


Fig. 10 Comparison of first harmonic of pressure fluctuation on bump wall - case B

6 Extension to three-dimensional flows

6.1 Numerical set up

In this part, results are discussed by the means of three-dimensional numerical computations. Available experimental data from Bron [13] are used for validation purpose. A single operating point corresponding to Tab. 3 was retained. The excitation frequency of back pressure fluctuation was set to 500 Hz.

	P_t^{in}	P_s^{out}	T_t^{in}	δP_s
B	160 kPa	106 kPa	303 K	2.12 kPa

Table 3 Description of operating point for three-dimensional unsteady computation with a frequency equal to 500 Hz

The whole numerical set up of previous two-dimensional studies was re-used. The 3D grid was generated by extruding the two-dimensional grid in the spanwise direction. Half of the nozzle is simulated to reduce computational cost by using a symmetry boundary condition.

6.2 Steady state results

Fig. 11 shows the three-dimensional structure of the steady state flow. A shockwave is located over the bump followed by a central separation. But, some phenomena that could not be captured through previous two-dimensional computation are now visible like corner separations due to thickening of side walls boundary layers. This greatly modifies the available section for the free flow and moves upstream the shock-wave compared to two-dimensional simulations. In order to predict the closest possible steady solution to experimental data, these structures have to be taken into account. Thus, a special interest was paid to inlet conditions (boundary layer) as well as outlet pressure setting.

As shown on Fig. 12, a good agreement was obtained on steady pressure distribution at different spanwise positions. Only the central separation seems to be underestimated, leading

to a shock position which is slightly downstream of the experimental one at mid-span. Moreover, this difference may also originate from small unsteadiness of the shockwave and limitation of our turbulence model. Nevertheless, we could expect a fair comparison of predicted and experimental unsteady behavior.

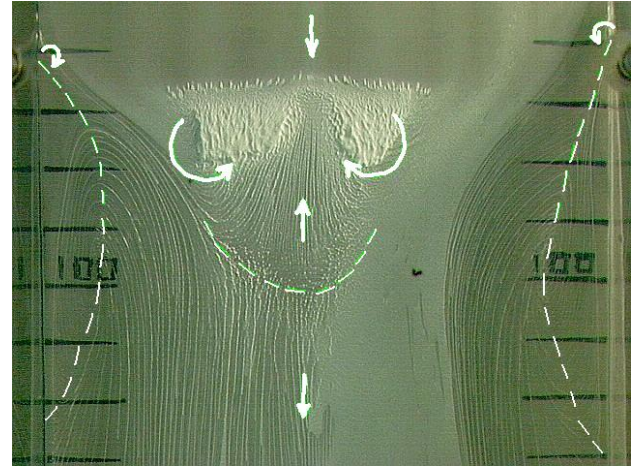


Fig. 11 Experimental oil visualization of steady state flow structure (top view from BRON [13]) - case B

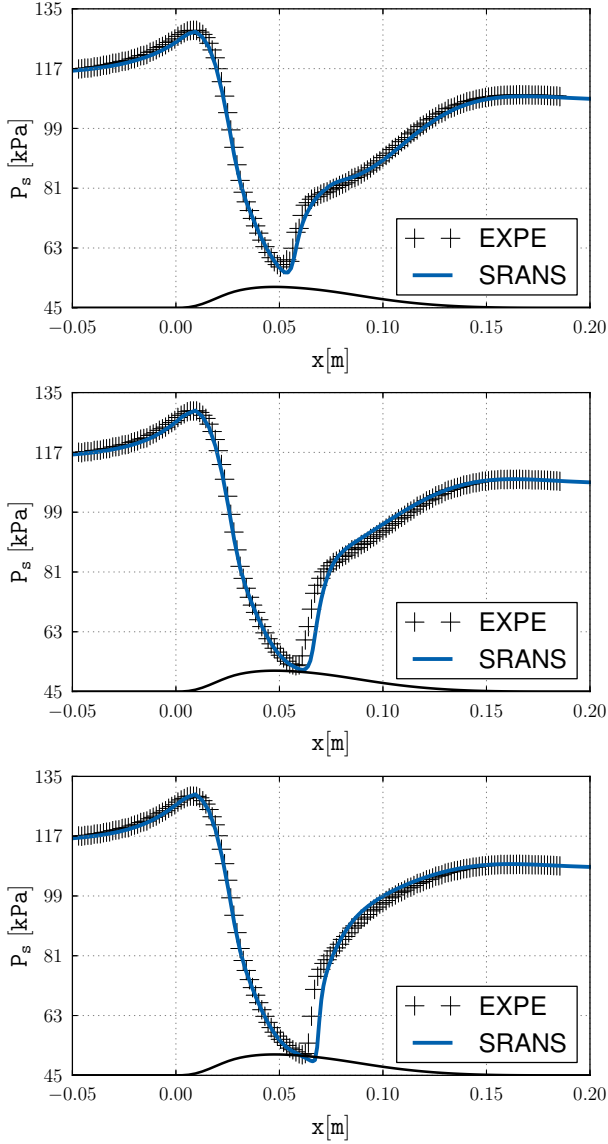


Fig. 12 Pressure distribution at 10%, 25% and 50% spanwise

6.3 LRANS computations of back-pressure fluctuations

Now, the performances of the LRANS method is evaluated. In particular, the influence of turbulence assumptions : either frozen or harmonic is investigated. Results were computed using Turb’Lin with the hypothesis of a back pressure plane wave. As a consequence, viscous effects of boundary layers at the fluctuating outlet were neglected.

A comparison of the unsteady pressure distribution over the bump with experimental data is presented in Figs. 13, 14 and 15 for three differ-

ent slices.

Since non-linearities are important in the regions of shockwave impact and separation, the frozen turbulence hypothesis failed completely. On the opposite, harmonic turbulence provides a really good agreement in terms of phase and normalized amplitude. At 10% spanwise, the amplitude was underestimated probably because of the viscous coupling with side wall was not correctly taken into account. In LRANS computations, peaks of pressure amplitude are located slightly downstream regarding experimental data. A possible explanation is that the shockwave position is not located correctly in the steady state flow.

From a physical point of view, the back-wave pressure fluctuation propagates quite homogeneously between $x = 0.13m$ and $x = 0.2m$ since phase and amplitude behave similarly whatever the span-wise position.

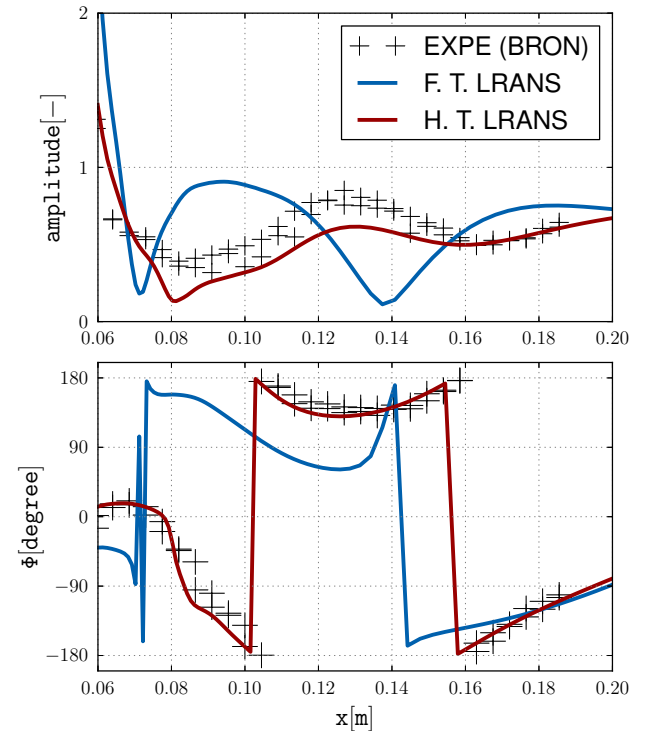


Fig. 13 Comparison of normalized pressure fluctuations at 10 % spanwise

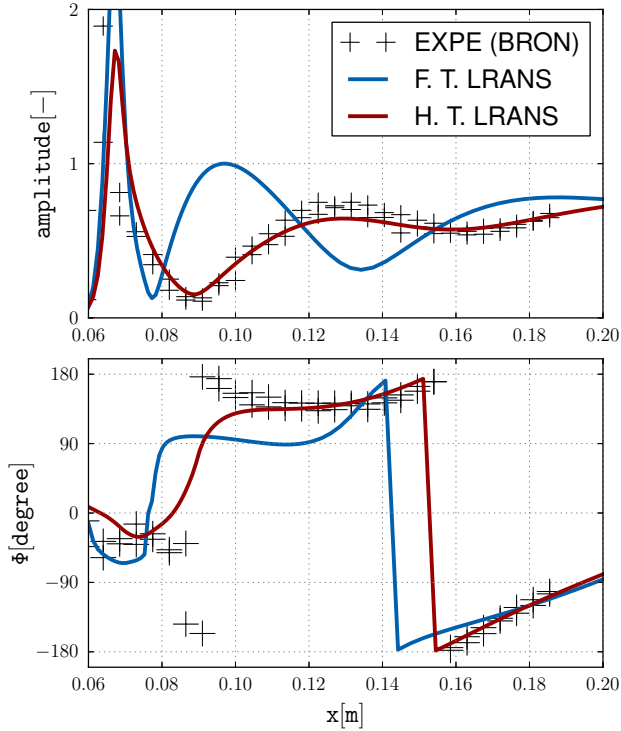


Fig. 14 Comparison of normalized pressure fluctuations at 25 % spanwise

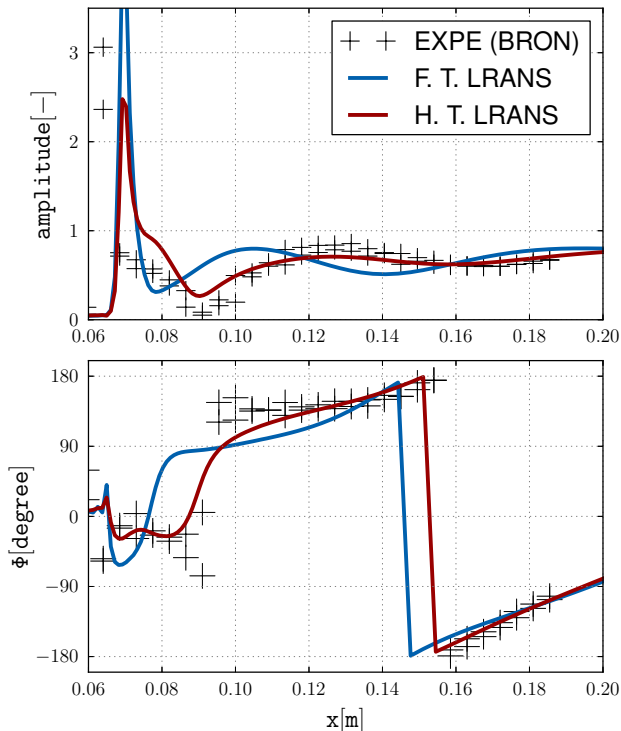


Fig. 15 Comparison of normalized pressure fluctuations at 50 % spanwise

7 Conclusion

A Linearized Reynolds Averaged Navier-Stokes solver, Turb’Lin, was successfully applied to the prediction of pressure fluctuations in a transonic nozzle. To this end the turbulence model of Wilcox was linearized using automatic differentiation in order to improve the accuracy of the LRANS method in regions characterized by strong non-linear phenomena. Intensive numerical studies were performed for two-dimensional configurations with an excitation frequency equal to 500 Hz. Dramatic improvements were observed for the case of strong shock-wave turbulent boundary layer interaction compared to two different LRANS method based on the assumption of frozen turbulence. These results were confirmed by the comparison of the H.T. LRANS method with an harmonic balance RSM RANS approach. Moreover, the benefit of using this time-linearized turbulence model was even more visible for three-dimensional results. Future work must be devoted to the study of the computational efficiency of the LRANS method (and the conditioning of the corresponding linear systems) for different values of the excitation frequency. Moreover the use of the Boussinesq law is questionable in the region of SW-TBL interaction. As a consequence, the linearization of time-lagged turbulence model represents a promising alternative to deal with forced oscillation of strongly separated flows.

7.1 Acknowledgements

This work was funded by the French National Agency of Research under the project ANR-08-2009 CapCAO (Parametrization aided optimized aeroelastic design).

Computational results were partially obtained using HPC resources from GENCI-CINES (Grant 2011-c2011026371)

References

- [1] D. Graham Holmes, Brian E. Mitchell, and Christopher B. Lorence, *Three dimensional linearized Navier-Stokes calculations for flutter and forced re-*

- sponse, Proceedings of the 8th International Symposium of Unstead Aerodynamics and Aeroelasticity of Turbomachines, 1997September, pp. 211–224.
- [2] W. S. Clark and K. C. Hall, *A time-linearized Navier-Stokes analysis of stall flutter*, Journal of Turbomachinery **122** (2000), no. 3, 467–476.
- [3] M. S. Campobasso and M. B. Giles, *Linear Harmonic Unsteady Flows in Turbomachines with Complex Iterative Solvers*, AIAA Journal **4705** (2005), 1–22.
- [4] A. K. Gopinath and Jameson A., *Time Spectral Method for Periodic Unsteady Computations over Two- and Three- Dimensional Bodies*, 43rd AIAA Aerospace Sciences Meeting and Exhibit, Reno [NV], Jan. 10 - 13, 2005.
- [5] J.P. Thomas, E.H. Dowell, and K.C. Hall, *A harmonic balance approach for modeling three-dimensional nonlinear unsteady aerodynamics and aeroelasticity*, American Society of Mechanical Engineers, Applied Mechanics Division (AMD) **253** (2002), no. 2, 1323–1334.
- [6] D. C. Wilcox, *Turbulence modeling for CFD*, 1st edition, , DCW Industries, Inc., 1993.
- [7] L. Smati, S. Aubert, P. Ferrand, and F. Massao, *Comparison of numerical schemes to investigate blade flutter*, Proceedings of the 8th International Symposium of Unstead Aerodynamics and Aeroelasticity of Turbomachines, 1997.
- [8] L. Smati, S. Aubert, and P. Ferrand, *Numerical study of unsteady shock motion to understand transonic flutter*, Proceedings of Euromech 349 on Simulation of fluid-structure interaction in aeronautics, 1996.
- [9] N.P. Waterson and H. Deconinck, *Design principles for bounded higher-order convection schemes - a unified approach*, Journal of Computational Physics **224** (2007), no. 1, 182–207.
- [10] J-C Chassaing, G. A. Gerolymos, and J-G Jérémiasz, *GMRES Solution of Compressible Linearized Navier-Stokes Equations without Pseudo-Time-Marching*, 44th AIAA Aerospace Sciences Meeting, 2006jan.
- [11] S. Aubert, J. Tournier, M. Rochette, J. Blanche, M. N’Diaye, S. Melen, M. Till, and P. Ferrand, *Optimization of a gas mixer using a new parametric flow solver*, ECCOMAS Computational Fluid Dynamics Conference, 2001, pp. 17.
- [12] S. Moreau, S. Aubert, M. N’Diaye, P. Ferrand, J. Tournier, and M. Rochette, *Parametric study of a fan blade cascade using a new parametric flow solver Turb’Opty*, ASME Joint US-European Fluids Engineering Conference, 2002, pp. 10.
- [13] O. Bron, *Numerical and experimental study of the Shock-Boundary Layer Interaction in Transonic Unsteady Flow*, Ph.D. Thesis, 2004.
- [14] P. Ferrand O. Bron and T. Fransson, *Experimental and numerical study of nonlinear interactions in two-dimensional transonic nozzle flow*, Unsteady aerodynamics, aeroacoustics and aeroelasticity of turbomachines, 2006, pp. 463–481.
- [15] G.A. Gerolymos, E. Sauret, and I. Vallet, *Contribution to single-point-closure Reynolds-stress modelling of inhomogeneous flow*, Theoretical and Computational Fluid Dynamics **17** (2004), 407–431.
- [16] G.A. Gerolymos and I. Vallet, *Implicit Meanflow-Multigrid Algorithms for Reynolds-Stress Model Computation of 3-D Anisotropy-Driven and Compressible Flows*, IJNMF **61** (2009), 185–219.
- [17] J.-C. Chassaing, G.A. Gerolymos, and I. Vallet, *Reynolds-Stress Model Dual-Time-Stepping Computation of Unsteady 3-D Flows*, AIAA Journal **41** (2003), 1882–1894.

7.2 Copyright Statement

The authors confirm that they, and/or their company or organization, hold copyright on all of the original material included in this paper. The authors also confirm that they have obtained permission, from the copyright holder of any third party material included in this paper, to publish it as part of their paper. The authors confirm that they give permission, or have obtained permission from the copyright holder of this paper, for the publication and distribution of this paper as part of the ICAS2012 proceedings or as individual off-prints from the proceedings.